

LOPR: Latent Occupancy PRediction using Generative Models

Bernard Lange, Masha Itkina, and Mykel J. Kochenderfer

Department of Aeronautics and Astronautics
Stanford University
United States
{blange, mitkina, mykel}@stanford.edu

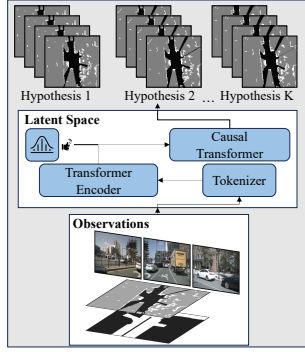
Abstract: Environment prediction frameworks are integral for autonomous vehicles, enabling safe navigation in dynamic environments. LiDAR generated occupancy grid maps (L-OGMs) offer a robust bird’s eye-view scene representation that facilitates joint scene predictions without relying on manual labeling unlike commonly used trajectory prediction frameworks. Prior approaches have optimized deterministic L-OGM prediction architectures directly in grid cell space. While these methods have achieved some degree of success in prediction, they occasionally grapple with unrealistic and incorrect predictions. We claim that the quality and realism of the forecasted occupancy grids can be enhanced with the use of generative models. We propose a framework that decouples occupancy prediction into: representation learning and stochastic prediction within the learned latent space. Our approach allows for conditioning the model on other available sensor modalities such as RGB-cameras and high definition maps. We demonstrate that our approach achieves state-of-the-art performance and is readily transferable between different robotic platforms on the real-world NuScenes, Waymo Open, and a custom dataset we collected on an experimental vehicle platform.

Keywords: Occupancy Prediction, Autonomous Driving, Generative Models

1 Introduction

Accurate environment prediction algorithms are essential for autonomous vehicle (AV) navigation in urban settings. Experienced drivers understand scene semantics and recognize the intents of other agents to anticipate their trajectories and safely navigate to their destination. To replicate this process in AVs and other robotic platforms, many environment prediction approaches have been proposed, employing different environment representations and modeling assumptions [1–9].

The modern AV stack comprises several sequential modules trained independently on labeled data. For environment reasoning, object-based prediction algorithms are commonly used [4, 6, 7, 10], which rely on perception systems to create a vectorized representation of the scene with pre-defined agents and environmental features. However, this approach has multiple limitations. 1) It generates marginalized future trajectories for individual agents, rather than a holistic scene prediction which complicates the integration with planning modules [11]. 2) Their reliance on labeled data, sourced either manually or from off-board perception systems [12, 13], diverges from on-board noisy detections. 3) They do not take any sensor measurements into account and depend solely on object detection algorithms which can fail in suboptimal conditions [14, 15]. These approaches also exclude social and topological cues that humans naturally perceive, emphasizing the importance of end-to-end perception-prediction learning [16]. The current drawbacks render the AV stack susceptible to cascading failures, and can lead to poor generalization to unforeseen scenarios. These limitations underscore the need for alternative end-to-end, self-supervised environment modeling approaches.



Method	Rep.	Maps	Cam.	Partial obs.	Stochast.	Prediction Type
Chai et al. [6]	Vector	✓	✗	✗	GMM	Per-agent
Ivanovic et al. [5]	Vector	✓	✗	✗	GMM	Per-agent
Gu et al. [22]	Vector	✓	✗	✗	Goal	Per-agent
Nayakanti et al. [16]	Vector	✓	✗	✗	GMM	Per-agent
Shi et al. [23]	Vector	✓	✗	✗	GMM	Per-agent
Itkina et al. [1]	L-OGM	✗	✗	✓	✗	Scene
Lange et al. [3]	L-OGM	✗	✗	✓	✗	Scene
Toyungyernsub et al. [24]	L-OGM	✗	✗	✓	✗	Scene
Mahjourian et al. [8]	V-OGM	✓	✗	✗	✗	Scene
Mersch et al. [25]	PCL	✗	✗	✓	✗	Scene
Wu et al. [26]	PCL	✓	✓	✓	✗	Scene
LOPR (ours)	L-OGM	✓	✓	✓	Variat.	Scene

Representations and prediction types in common approaches

Figure 1: (Left) Latent Occupancy PRediction (LOPR). We decouple the prediction task into task-independent representation learning, and task-dependent prediction in the latent space. (Right) Comparison with other approaches in terms of representation type, sensors, stochasticity assumptions, and prediction type. Only LOPR makes stochastic predictions of the scene conditioned on all sensors without the need for manually labelled data.

Given these challenges, occupancy grid maps generated from LiDAR measurements (L-OGMs) have gained popularity as a form of scene representation for prediction. This popularity is due to their minimal data preprocessing requirements, eliminating the need for manual labeling, ability to model the joint prediction of the scene with an arbitrary number of agents (including interactions between agents), and robustness to partial observability and detection failures [1–3, 17]. In addition, the sole requirement for their deployment is a LiDAR sensor, simplifying transfer between different platforms. Our focus is on end-to-end ego-centric L-OGM prediction generated using uncertainty-aware occupancy state estimation approaches [18]. Due to its generality and ability to scale with unlabeled data, we hypothesize that such an L-OGM prediction framework could also serve as a pre-training objective, i.e. a foundational mode, for supervised tasks such as trajectory prediction.

The task of OGM prediction is typically approached similarly to video prediction, by framing the problem as self-supervised sequence-to-sequence learning. In this approach, a scenario is dissected into a history sequence and a target prediction sequence. ConvLSTM-based architectures [19] have been used in previous work for this task due to their ability to handle the spatiotemporal representation of inputs and outputs [1–3, 20, 21]. These approaches are optimized end-to-end in grid cell space, do not account for the stochasticity present in the scene, and neglect other available sensor modalities, e.g. RGB cameras and high definition (HD) maps. As a result, they suffer from blurry predictions, especially at longer time horizons. We propose a prediction framework that reasons over potential futures in the latent space of generative models. It is trained on sensor modalities such as L-OGMs, 2D RGB cameras, and maps without the need for manual labeling. We illustrate our framework in Fig. 1 and compare it with other methods.

Recent work has shown generative models can produce high-quality [27, 28] and controllable [29–31] samples. In robotics, generative models have been used to find compact representations of images in planning [32–34], control [35–37], and simulation [38]. We claim that generative models are similarly capable of accurately encoding and decoding L-OGMs, alongside providing a controllable latent space for high-quality predictions. We employ a generative model to learn a low-dimensional latent space, which encodes the features needed to generate realistic predictions and makes use of available input modalities, such as L-OGM, RGB camera, and map-based observations. We then train a stochastic prediction network in this latent space to capture the dynamics of the scene.

Existing object-based methods use a vectorized representation to predict trajectories [5, 6, 22] or vectorized OGMs (V-OGMs) [8], overlooking important perceptual cues in their predictions. Prior L-OGM-based works [1, 3, 25] do not use available sensor modalities, and consider only deterministic predictions. Our framework addresses these weaknesses in the following contributions:

- We introduce a framework named **Latent Occupancy PRediction (LOPR)**, which performs stochastic L-OGM prediction in the latent space of a generative architecture conditioned on other available sensor modalities, like RGB cameras and maps.

- Through experiments on NuScenes [39] and the Waymo Open Dataset [40], we show that LOPR outperforms SOTA OGM prediction methods qualitatively and quantitatively.
- We demonstrate that LOPR can be conveniently transferred between different robotic platforms by additionally evaluating our framework on a custom robotic dataset.

2 Related Work

OGM Prediction: The majority of prior work in OGM prediction generates OGMs with LiDAR measurements (L-OGMs) and uses an adaptation on the recurrent neural network (RNN) with convolutions. Dequaire et al. [41] applied a Deep Tracking approach [42] to track objects through occlusions and predict future binary OGMs with an RNN and a spatial transformer [43]. Schreiber et al. [20] provided dynamic occupancy grid maps (DOGMas) with cell-wise velocity estimates as input to a ConvLSTM [19] for environment prediction from a stationary platform. Schreiber et al. [21] extended this work to forecast DOGMas in a moving ego-vehicle setting. Mohajerin and Rohani [17] applied a difference learning approach to predict OGMs as seen from the coordinate frame of the first observed time step. Itkina et al. [1] used the PredNet ConvLSTM architecture [44] to achieve ego-centric OGM prediction. Lange et al. [3] reduced the blurring and the gradual disappearance of dynamic obstacles in the predicted grids by developing an attention augmented ConvLSTM mechanism. Concurrently, Toyungyernsub et al. [2] addressed obstacle disappearance with a double-prong framework assuming knowledge of the static and dynamic obstacles. Predicted OGMs often lack agent identity information. Mahjourian et al. [8] addressed this by exploiting occupancy flow estimates to trace back the agent identities from the observed OGM frames. They used upstream perception detections to generate OGMs with vectorized representations (V-OGMs) and hence require manual labeling. Unlike prior work, we perform stochastic OGM predictions in the latent space of generative models of all available sensors without any manual labeling.

Representation Learning in Robotics: The objective of representation learning is to identify a low-dimensional and disentangled representation that makes it easier to achieve the desired performance on a task. Many robotics applications are inspired by the seminal papers on the autoencoder (AE) [45–47], the variational autoencoder (VAE) [29], and the generative adversarial network (GAN) [27]. Ha and Schmidhuber [32] proposed a World Model, where they used a VAE to compress observations and maximize the expected cumulative reward. Kim et al. [38] applied the World Model to neural network simulation for autonomous driving, where they merged the VAE [29] and StyleGAN [28] to increase fidelity of the generated scenes. Similarly, latent spaces have been used in a plethora of other planning and control approaches to learn latent dynamics from pixels [36, 37, 48–50], generate fully imagined trajectories [51], model multi-agent interactions [33], learn competitive policies through self-play [34], imagine goals in goal-conditioned policies [52, 53], and perform meta- and offline reinforcement learning [54, 55]. Diffusion-based generative models [56–59] are increasingly gaining traction due to their high sampling quality. However, their computationally intensive sampling process poses a significant obstacle for real-time robotic applications in the context of perceptual generation. In video prediction tasks, variational and adversarial components have been incorporated into the architecture to capture data stochasticity [60] and improve the realism of the forecasted frames [61], respectively. Since then, large-scale architectures (over 300 million parameters) [62, 63] have been developed for general video prediction, which are not real-time capable on robot hardware. We present the first method, to our knowledge, that performs stochastic L-OGM prediction with transformers entirely in the latent space of a generative model while remaining real-time feasible and parameter efficient (less than 4 million parameters).

3 LOPR: Latent Occupancy PRediction

We propose the Latent Occupancy PRediction (LOPR) model, a framework designed to generate stochastic scene predictions in the form of OGMs. The model uses representations provided by sensor modalities, such as LiDAR-generated OGMs, RGB cameras, and maps. It does not require any manually labeled data and can be deployed on any robot equipped with at least a LiDAR sen-

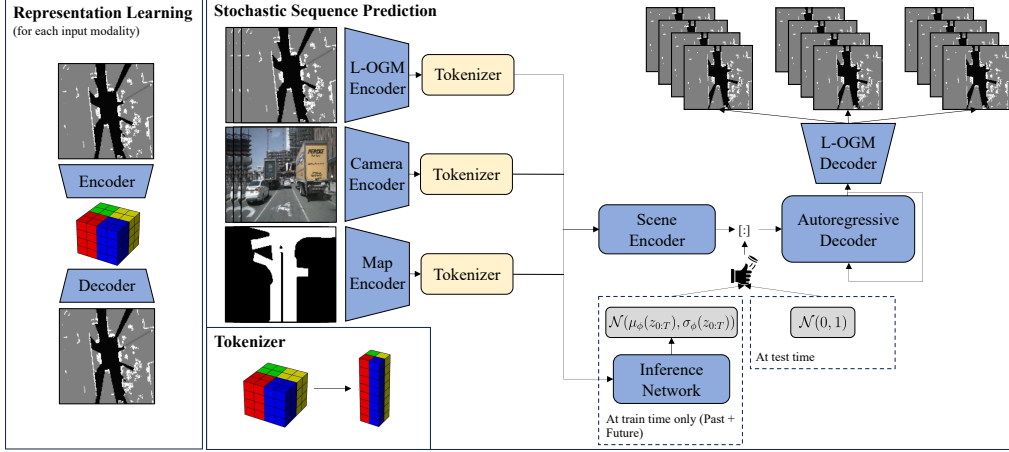


Figure 2: The illustration shows the LOPR framework which consists of (1) representation learning and (2) stochastic sequence prediction. In the representation learning stage, we train an encoder and decoder in an unsupervised manner. In the sequence prediction stage, we convert our OGM dataset to the low-dimensional representation, and perform training entirely in the latent space of our pre-trained generative model.

sor. A visualization of the framework is provided in Fig. 2. The model separates the prediction task into (1) learning the environment representation and (2) making predictions in the latent space of a generative model. In the representation learning phase, a VAE-GAN is trained to acquire a pre-trained latent space of rasterized sensor measurements. During the prediction stage, an autoregressive transformer [64] network is trained within the pre-trained latent space to predict future OGMs. It operates over patches of each latent vector to reduce the dimensionality of the prediction network and employs a series of auxiliary tasks incorporating various sequence masking strategies during training to further improve performance.

3.1 Representation Learning

In the first stage of training, we acquire a pre-trained latent space of all input modalities by training an encoder \mathcal{E} and a decoder \mathcal{D} . Given the input modality $x \in \mathbb{R}^{C \times W \times H}$, the encoder outputs a low-dimensional latent vector $z \in \mathbb{R}^{c \times h \times w}$, and the decoder maps the latent vector to a reconstruction $\hat{x} \in \mathbb{R}^{C \times W \times H}$. The framework is trained using a combination of perceptual loss [65], Kullback-Leibler (KL) regularization [29], patch-based adversarial losses [66] and path regularization [28]:

$$L_{\text{VAEGAN}} = \min_{\mathcal{E}, \mathcal{D}} \max_{\psi} (L_{\text{LPIPS}}(x, \mathcal{D}(\mathcal{E}(x))) - \gamma L_{\text{adv}}(\mathcal{D}(\mathcal{E}(x))) + \beta L_{\text{KL}}(x; \mathcal{E}, \mathcal{D}) + L_{\text{reg}}). \quad (1)$$

We employ the adversarial loss to increase the visual fidelity of the generated samples, KL regularization to encourage the posterior $q(z | x)$ to be clustered close the prior $p(z) = \mathcal{N}(0, I)$.

3.2 Stochastic Sequence Prediction

Given the pre-trained latent space of our sensor data, we train a stochastic sequence prediction network that receives a history of observations and outputs a distribution of potential future scenarios $p_{\theta}(z_{P:T} | z_{0:P})$, where $z_{0:P}$ represents compressed observations over P timesteps, T signifies the total sequence length, and θ are the network weights. To simplify notation, we assume an abuse of notation in that when z_t corresponds to an observation, it includes all sensor modalities; conversely, when referring to the future, it includes only the OGM representation. The environment prediction task is inherently multimodal, and the latent vectors contributing to this stochasticity are unobservable. Drawing from prior work on video prediction [60], we introduce a latent vector $z_{\text{stoch}} \sim p(z_{\text{stoch}})$ to encapsulate this stochasticity and extend our model to $p_{\theta}(z_{P:T} | z_{0:P}, z_{\text{stoch}})$. During training, we extract the true posterior $p(z_{\text{stoch}} | z_{0:T})$ using an inference network $z_{\text{stoch}} \sim q_{\phi}(z_{\text{stoch}} | z_{0:T})$, while at test time, we sample from a pre-defined prior $p(z_{\text{stoch}})$. The framework

is optimized using the variational lower bound [29]:

$$\mathcal{L}(\mathbf{z}) = -\mathbb{E}_{q_\phi(z_{stoch} | z_{0:T})} [\log p_\theta(z_{P:T} | z_{0:P}, z_{stoch})] + D_{KL}(q_\phi(z_{stoch} | z_{0:T}) || p(z_{stoch})), \quad (2)$$

where D_{KL} is the Kullback-Leibler divergence, and $p(z_{stoch})$ is standard Gaussian [60, 61, 67, 68].

We implement our model using a transformer-based architecture, comprised of a scene encoder $\mathcal{P}_{encoder,\theta}$, an inference network \mathcal{Q}_ϕ , and an autoregressive decoder $\mathcal{P}_{decoder,\theta}$. In all transformation-based operations, positional information is provided through a sinusoidal positional encoding [64]. To reduce the number of parameters required in the attention layer for processing each token and to facilitate spatial attention, each latent vector $z \in \mathbb{R}^{c \times h \times w}$ is reshaped along the spatial dimensions to a sequence of smaller cuboids $z \in \mathbb{R}^{k^2 c \times \frac{h}{k} \times \frac{w}{k}}$. This is followed by spatial partitioning. A single latent vector z thus generates a sequence of $\frac{hw}{k^2}$ tokens, each of length $k^2 c$.

The scene encoder and inference network are implemented using a transformer architecture, wherein each token can attend to every other token. The scene encoder takes in tokens generated with latent vectors for all sensor modalities and outputs scene contexts $scene_{emb} \in \mathbb{R}^{kc^2}$. The posterior network takes in the all OGM latent vectors, including the future ones, and outputs parameters for the Gaussian distribution μ and σ , used for z_{stoch} :

$$scene_{emb} = \mathcal{P}_{encoder,\theta}(z_{0:P}) \quad (3)$$

$$z_{stoch} \sim \mathcal{N}(\mu_\phi(z_{0:T}), \sigma_\phi(z_{0:T})). \quad (4)$$

Both $scene_{emb}$ and z_{stoch} are concatenated along the temporal dimension and serve as memory tokens to $\mathcal{P}_{decoder,\theta}$, which is implemented using a causal transformer to generate predictions:

$$z_t = \mathcal{P}_{decoder,\theta}(z_{0:t-1}, mem = [scene_{emb}, z_{stoch}]) \quad (5)$$

In the final step, the predicted compressed representations are concatenated, reshaped back to their original dimensions, and then fed into the pretrained decoder \mathcal{D} to produce the OGM predictions.

4 Experiments

We analyze our proposed framework based on its pre-trained latent space and how well it performs on environment prediction tasks. We also consider how additional sensor modalities affect the prediction quality. Our framework is tested against prior methods in L-OGM forecasting and top-performing sequence-to-sequence video prediction models of similar scale. We use the open-source datasets, NuScenes [39] and the Waymo Open Dataset [40], for training and evaluation. To demonstrate the versatility of our framework, we evaluate our models on a custom urban robotic dataset. Our results show that LOPR reaches SOTA performance in the prediction task. Our code with additional visualizations is available [here](#).

4.1 Datasets

NuScenes Dataset [39] is an AV dataset collected in Boston and Singapore. The autonomous vehicle sensor suite includes 6 12Hz RGB cameras, a 20Hz 32-beam LiDAR, GPS, and an IMU. It also provides rasterized maps featuring drivable areas, stop signs, and pedestrian crossings.

Waymo Open Dataset is an AV dataset compiled in San Francisco, Phoenix, and Mountain View. The data collection platform incorporates 5 LiDARs, 5 RGB cameras, GPS, and an IMU, with samples collected at 10 Hz. Maps are provided in vectorized form.

Custom Robot Platform Dataset: To demonstrate the transferability of our framework, we collect a small dataset comprising 20 scenes, each 20 seconds long, in an urban setting with a mobile robotic platform equipped with Velodyne’s HDL-32E 32-beam LiDAR. Within this dataset, we observe interactions with cars, buses, cyclists, and pedestrians.

Data Representation: We generate OGMs using a ground-segmented LiDAR point cloud. The OGM dimensions are $H \times W = 128 \times 128$ with a 0.3 m resolution, corresponding to a $42.7\text{ m} \times 42.7\text{ m}$ grid. We downscale RGB images and maps to the same resolution. During the sequence prediction training phase, we provide 5 past OGMs (0.5 s) as observations alongside other sensor modalities, and predict for 15 frames (1.5 s) into the future at 10 Hz. For all open-source datasets, we adhere to the original dataset specification for the train-validation-test split.

4.2 Architecture and Training Details

Architectures: Our encoder and decoder employ a convolutional network with residual connections, and a latent vector $z \in \mathbb{R}^{64 \times 4 \times 4}$. The discriminator is multi-scale and multi-patch, following previous work [66, 69, 70]. We use a vanilla Transformer implementation provided in PyTorch [71].

Model Training: We trained the models using PyTorch Lightning 1.4.2 [71, 72]. We used the AdamW optimizer [73] with a learning rate of 4×10^{-4} . For representation learning, we used four NVIDIA V100 32 GB GPUs. The autoencoders were trained for 80k steps with a batch size of 128. We trained all prediction models on a Nvidia Titan RTX 24 GB GPU with 256 batch size.

4.3 Evaluation

Baselines: We benchmark against methods commonly used in L-OGM prediction, such as PredNet [1, 44] and TAAConvLSTM [3]. Due to their representational similarity to our approach, we also draw comparisons with available SOTA video prediction methods of similar scale like SimVP V2 [74], PredRNN V2 [75], and E3DLSTM [76]. We also introduce a baseline that uses the last observed frame as a prediction to assess how effectively the models capture the scene’s motion.

Quantitative Evaluation: We evaluate all models using the Image Similarity (IS) metric [77] across the 1.5 s and 3.0 s prediction and the accuracy of occupied cells at the end of the 3.0 s rollout. For stochastic predictions, we sample 10 predictions and evaluate the best-performing one. Similar to the mean squared error (MSE) used in trajectory prediction, we are interested in the relative distance errors between observed objects and predicted position of the object but in the discretized space. The IS metric captures the variations in predicted multi-future agent positions [3]. Commonly used precision-focused metrics, like MSE, penalize a missing moving agent significantly less than a predicted agent’s slight positional shift when compared with the ground truth [3]. The IS metric calculates the smallest Manhattan distance between two grid cells with the same thresholded occupancy. Its numerical evaluation is proportional to the discrepancy between predicted and observed positions and is notably high when an agent completely disappears. We also provide an accuracy of occupied cells at the end of the 3.0 s rollout to highlight the critical issue of vanishing moving objects, a common and prohibitive failure for safety-critical applications.

5 Results

5.1 Latent Space Analysis

The latent space trained in the representation learning stage is essential to facilitate accurate predictions. If an agent in the observed frames is lost during the encoding phase, the prediction network will have difficulties recovering this information, potentially leading to incorrect forecasting. We investigate the reconstruction performance qualitatively and quantitatively. Our framework successfully recovers each sensor modality’s observation from their respective low-dimensional representations as visualized in Fig. 3. We investigate the impact of KL regularization in Table 1. We observe that high KL regularization is needed for the L-OGM’s VAE-GAN to generate high quality predictions. The KL term induces better regularization and smoothness in the learned latent space, resulting in improved generalization. We hypothesize that predictions in the latent space will unavoidably incur some inaccuracies, and thus, will not perfectly correspond to the ground truth L-OGM data distribution. This better generalization is important when making predictions in the



Figure 3: Example reconstructions of OGMs, images, and maps from NuScenes.

latent space. We also report the reconstruction performance of camera and map observations. We did not observe significant impact of their regularization on the prediction task.

5.2 Prediction Task

We assess the predictive capabilities of LOPR in Table 2 and show its predictions in Figs. 4 and 5. We investigate the influence of stochasticity and the addition of other sensor modalities by evaluating deterministic and stochastic models conditioned only on L-OGMs, and another stochastic model conditioned on all available inputs. All LOPR variations notably outperform prior work in L-OGM prediction, as evidenced by the IS and accuracy metrics. The improvements become more pronounced with the integration of additional modalities and stochastic modeling. LOPR is also the only framework that markedly outperforms the simple baseline, which repeats the last observation, demonstrating its ability to capture the scene’s dynamics.

In Fig. 4, we visualize the predictions rolled out for 3.0 s into the future, i.e. beyond the prediction horizon used during training. LOPR produces high-quality, realistic predicted frames, supporting quantitative results. Dynamic objects are realistically propagated in the scene and the details of the static environment are maintained, unlike prior approaches [1, 3]. Fig. 5 presents varied prediction samples from challenging scenarios characterized by partial observability. Each sample captures a realistic plausible future rollout. Our framework is capable of inferring a previously unobserved agent entering the L-OGM. Our framework is the first, to the best of our knowledge, to successfully generate realistic stochastic OGM predictions conditioned on multi-modal sensor data.

Prior work that uses ConvLSTM-based architectures optimized for the spatiotemporal prediction task in grid cell space [1–3, 20] suffers from lack of sharpness and poor realism in their predictions. For example, occluded cells are often not preceded by occupied cells, making the frames physically incorrect, and forecasted L-OGMs gradually lose important details over the prediction horizon. Lack of sharpness eventually leads to the vanishing of moving objects and, hence, missing agents in the predictions [1, 3] and a low IS metric value. These failures are not present in LOPR’s predictions.

We also demonstrate successful transfer of our LOPR model trained on the NuScenes dataset to our custom robotic dataset in Table 2 and Fig. 4. The quantitative prediction performance on this dataset is comparable in magnitude to the other datasets, despite the data distribution shift. Thus, LOPR is able to successfully generalize beyond its training data distribution.

6 Limitations

Although decoupling the representation learning and prediction stages allows us to achieve high-quality OGM predictions empirically, LOPR relies on a well trained latent space that may not be tuned for prediction. If the latent encoding misses important scene information (such as moving agents), the prediction network will not be able to recover this information and fail to predict the agent. Furthermore, as any learned module in a safety-critical engineering system, like an AV, LOPR

Table 1: Impact of KL regularization during representation learning on LOPR’s performance in terms of reconstruction and a simplified prediction task using the NuScenes dataset. For all metrics, lower is better.

KL	OGM Recon. (IS)	OGM Prediction (IS)	Camera Recon. (MSE)	Map Recon. (MSE)
1×10^{-6}	3.51 ± 0.01	14.85 ± 0.72	2.21 ± 0.04	0.49 ± 0.04
1.0	1.71 ± 0.01	15.90 ± 0.34	2.89 ± 0.07	0.51 ± 0.06
4.0	1.75 ± 0.01	13.19 ± 0.42	3.12 ± 0.06	0.53 ± 0.07

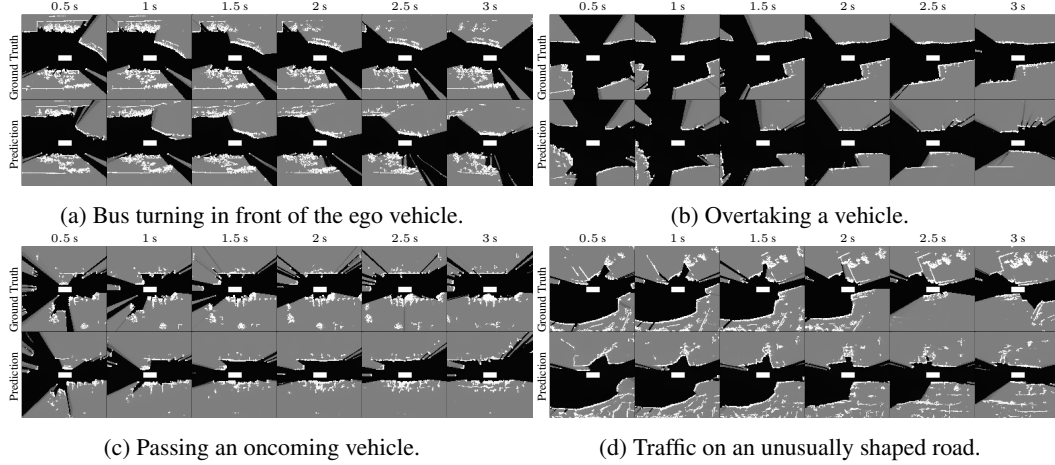


Figure 4: Predictions from NuScenes conditioned on L-OGM only. Ego vehicle is moving to the right. Moving objects are realistically propagated in the scene and the details of the static environment are maintained.

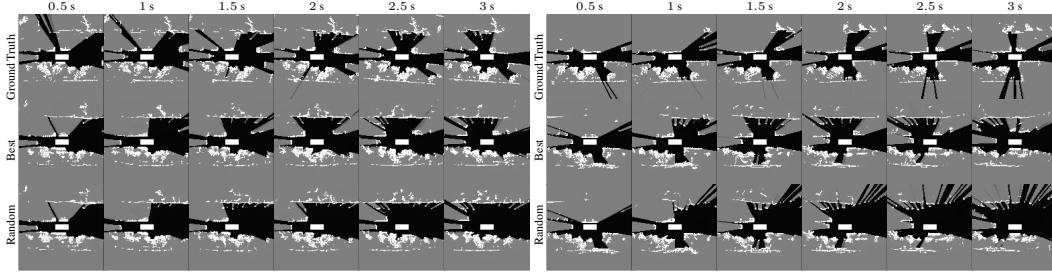


Figure 5: Comparison of best predictions and random predictions from NuScenes conditioned on L-OGM only. Our framework is capable of inferring a previously unobserved oncoming agent entering the L-OGM in both scenes and different variations of static environment.

would need to be tested rigorously against potential out-of-distribution (OOD) scenarios. LOPR does not currently identify OOD inputs that may cause failures. To enable such capability, we could adopt an approach for epistemic uncertainty estimation as proposed by Itkina and Kochenderfer [78].

7 Conclusion

In this paper, we proposed an L-OGM prediction framework, LOPR, that decouples representation and prediction learning. LOPR consists of a VAE-GAN-based generative model that learns an expressive low-dimensional latent space of available sensor modalities and a transformer-based stochastic prediction network that operates on the learned latent space. Our experiments show that LOPR achieves SOTA performance, qualitatively and quantitatively outperforming prior L-OGM approaches and video prediction architectures. We also demonstrate that our framework can be eas-

Table 2: NuScenes, Waymo Open Perception, and Custom Robotic dataset prediction results.

Model	NuScenes Dataset			Waymo Open Perception Dataset			Custom Robotic Dataset		
	IS _{5→15} (↓)	IS _{5→30} (↓)	Acc. (↑)	IS _{5→15} (↓)	IS _{5→30} (↓)	Acc. (↑)	IS _{5→15} (↓)	IS _{5→30} (↓)	Acc. (↑)
ED3LSTM [76]	8.25 ± 0.13	18.96 ± 1.59	0.13 ± 0.01	8.97 ± 0.21	41.05 ± 4.31	0.02 ± 0.01	12.83 ± 0.21	21.44 ± 1.76	0.16 ± 0.01
TAAConvLSTM [3]	6.90 ± 0.09	15.23 ± 3.94	0.14 ± 0.01	6.58 ± 0.42	21.96 ± 2.01	0.27 ± 0.02	18.57 ± 0.62	24.21 ± 1.90	0.15 ± 0.01
PredRNN V2 [75]	13.04 ± 0.24	79.95 ± 4.64	0.03 ± 0.01	11.85 ± 0.027	68.78 ± 6.06	0.11 ± 0.01	32.71 ± 0.76	94.54 ± 6.89	0.04 ± 0.01
Sim.VP V2 [74]	11.86 ± 0.19	54.09 ± 2.87	0.02 ± 0.01	8.77 ± 0.20	48.35 ± 3.57	0.06 ± 0.01	27.45 ± 0.98	64.22 ± 7.82	0.09 ± 0.01
PredNet [1, 44]	7.01 ± 0.14	13.89 ± 0.43	0.14 ± 0.01	6.92 ± 0.61	22.26 ± 1.32	0.35 ± 0.05	18.98 ± 0.85	23.54 ± 8.91	0.15 ± 0.01
Fixed Last Obs Frame	11.50 ± 0.14	14.41 ± 0.18	0.20 ± 0.01	10.35 ± 0.41	14.74 ± 0.54	0.38 ± 0.01	24.76 ± 0.94	31.81 ± 1.65	0.25 ± 0.01
Ours									
Deterministic (L-OGM)	8.09 ± 0.26	11.48 ± 1.38	0.40 ± 0.01	5.92 ± 0.63	12.49 ± 2.05	0.44 ± 0.02	11.87 ± 0.32	16.52 ± 4.91	0.34 ± 0.01
Stochastic (L-OGM)	7.22 ± 0.10	9.78 ± 0.34	0.59 ± 0.02	5.73 ± 0.65	12.32 ± 2.34	0.51 ± 0.07	10.43 ± 0.52	14.65 ± 3.76	0.49 ± 0.03
Stochastic (All)	7.01 ± 0.24	9.16 ± 0.68	0.61 ± 0.01	5.85 ± 0.31	12.18 ± 2.62	0.51 ± 0.01	N/A	N/A	N/A

ily deployed on any robotic platform equipped with a LiDAR sensor, in contrast to most trajectory prediction approaches, which would require addressing compounding data distribution errors across modules and changes in sensor positioning. We hope that learnings from this framework open new research avenues in the L-OGM prediction field. In future work, we will explore how LOPR can be extended to perform 3D occupancy prediction, be applied to other tasks, such as occlusion inference [79] and path planning [80], and serve as a pre-training task for supervised models, such as trajectory prediction.

Acknowledgments

This project was made possible by funding from the Ford-Stanford Alliance.

References

- [1] M. Itkina, K. Driggs-Campbell, and M. J. Kochenderfer. Dynamic environment prediction in urban scenes using recurrent representation learning. In *International Conference on Intelligent Transportation Systems (ITSC)*, pages 2052–2059. IEEE, 2019.
- [2] M. Toyungyernsub, M. Itkina, R. Senanayake, and M. J. Kochenderfer. Double-prong ConvLSTM for spatiotemporal occupancy prediction in dynamic environments. In *International Conference on Robotics and Automation (ICRA)*, pages 13931–13937. IEEE, 2021.
- [3] B. Lange, M. Itkina, and M. J. Kochenderfer. Attention augmented ConvLSTM for environment prediction. In *International Conference on Intelligent Robots and Systems (IROS)*, pages 1346–1353. IEEE, 2020.
- [4] T. Salzmann, B. Ivanovic, P. Chakravarty, and M. Pavone. Trajectron++: Dynamically-feasible trajectory forecasting with heterogeneous data. In *European Conference on Computer Vision (ECCV)*, pages 683–700. Springer, 2020.
- [5] B. Ivanovic, A. Elhafsi, G. Rosman, A. Gaidon, and M. Pavone. MATS: An interpretable trajectory forecasting representation for planning and control. In *Conference on Robot Learning (CoRL)*, 2021.
- [6] Y. Chai, B. Sapp, M. Bansal, and D. Anguelov. MultiPath: Multiple probabilistic anchor trajectory hypotheses for behavior prediction. In *Conference on Robot Learning (CoRL)*, 2020.
- [7] C. Tang and R. R. Salakhutdinov. Multiple futures prediction. In *Advances in Neural Information Processing Systems (NeurIPS)*, pages 15398–15408, 2019.
- [8] R. Mahjourian, J. Kim, Y. Chai, M. Tan, B. Sapp, and D. Anguelov. Occupancy flow fields for motion forecasting in autonomous driving. *IEEE Robotics and Automation Letters*, 7(2): 5639–5646, 2022.
- [9] J. Ngiam, B. Caine, V. Vasudevan, Z. Zhang, H.-T. L. Chiang, J. Ling, R. Roelofs, A. Bewley, C. Liu, A. Venugopal, D. J. Weiss, B. Sapp, Z. Chen, and J. Shlens. Scene Transformer: A unified architecture for predicting future trajectories of multiple agents. In *International Conference on Learning Representations (ICLR)*, 2021.
- [10] H. Zhao, J. Gao, T. Lan, C. Sun, B. Sapp, B. Varadarajan, Y. Shen, Y. Shen, Y. Chai, C. Schmid, C. L. Li, and D. Anguelov. TNT: Target-driven trajectory prediction. In *Conference on Robot Learning (CoRL)*, 2020.
- [11] Y. Chen, B. Ivanovic, and M. Pavone. Scept: Scene-consistent, policy-based trajectory predictions for planning. In *Computer Society Conference on Computer Vision and Pattern Recognition (CVPR)*, pages 17103–17112, 2022.

- [12] S. Ettinger, S. Cheng, B. Caine, C. Liu, H. Zhao, S. Pradhan, Y. Chai, B. Sapp, C. R. Qi, Y. Zhou, et al. Large scale interactive motion forecasting for autonomous driving: The waymo open motion dataset. In *International Conference on Computer Vision (ICCV)*, pages 9710–9719, 2021.
- [13] C. R. Qi, Y. Zhou, M. Najibi, P. Sun, K. Vo, B. Deng, and D. Anguelov. Offboard 3d object detection from point cloud sequences. In *Computer Society Conference on Computer Vision and Pattern Recognition (CVPR)*, pages 6134–6144, 2021.
- [14] H. Delecki, M. Itkina, B. Lange, R. Senanayake, and M. J. Kochenderfer. How do we fail? stress testing perception in autonomous vehicles. In *International Conference on Intelligent Robots and Systems (IROS)*, pages 5139–5146. IEEE, 2022.
- [15] M. Dreissig, D. Scheuble, F. Piewak, and J. Boedecker. Survey on lidar perception in adverse weather conditions. In *IEEE Transactions on Intelligent Vehicles*, pages 1–8, 2023.
- [16] N. Nayakanti, R. Al-Rfou, A. Zhou, K. Goel, K. S. Refaat, and B. Sapp. Wayformer: Motion forecasting via simple & efficient attention networks. In *International Conference on Robotics and Automation (ICRA)*, pages 2980–2987, 2023.
- [17] N. Mohajerin and M. Rohani. Multi-step prediction of occupancy grid maps with recurrent neural networks. In *Computer Society Conference on Computer Vision and Pattern Recognition (CVPR)*, pages 10600–10608. IEEE, 2019.
- [18] A. Elfes. Using occupancy grids for mobile robot perception and navigation. *Computer*, 22(6):46–57, 1989.
- [19] S. Xingjian, Z. Chen, H. Wang, D.-Y. Yeung, W.-K. Wong, and W.-c. Woo. Convolutional LSTM network: A machine learning approach for precipitation nowcasting. In *Advances in Neural Information Processing Systems (NeurIPS)*, pages 802–810, 2015.
- [20] M. Schreiber, S. Hoermann, and K. Dietmayer. Long-term occupancy grid prediction using recurrent neural networks. In *International Conference on Robotics and Automation (ICRA)*, pages 9299–9305. IEEE, 2019.
- [21] M. Schreiber, V. Belagiannis, C. Gläser, and K. Dietmayer. Dynamic occupancy grid mapping with recurrent neural networks. In *International Conference on Robotics and Automation (ICRA)*, pages 6717–6724. IEEE, 2021.
- [22] J. Gu, C. Sun, and H. Zhao. Densetnt: End-to-end trajectory prediction from dense goal sets. In *International Conference on Computer Vision (ICCV)*, pages 15303–15312, 2021.
- [23] S. Shi, L. Jiang, D. Dai, and B. Schiele. Motion transformer with global intention localization and local movement refinement. In *Advances in Neural Information Processing Systems (NeurIPS)*, 2022.
- [24] M. Toyungyernsub, E. Yel, J. Li, and M. J. Kochenderfer. Dynamics-aware spatiotemporal occupancy prediction in urban environments. In *International Conference on Intelligent Robots and Systems (IROS)*, pages 10836–10841. IEEE, 2022.
- [25] B. Mersch, X. Chen, J. Behley, and C. Stachniss. Self-supervised point cloud prediction using 3d spatio-temporal convolutional networks. In *Conference on Robot Learning (CoRL)*, pages 1444–1454, 2022.
- [26] P. Wu, S. Chen, and D. N. Metaxas. Motionnet: Joint perception and motion prediction for autonomous driving based on bird’s eye view maps. In *International Conference on Computer Vision (ICCV)*, pages 11385–11395, 2020.

- [27] I. Goodfellow, J. Pouget-Abadie, M. Mirza, B. Xu, D. Warde-Farley, S. Ozair, A. Courville, and Y. Bengio. Generative adversarial nets. *Advances in Neural Information Processing Systems (NeurIPS)*, 27, 2014.
- [28] T. Karras, S. Laine, M. Aittala, J. Hellsten, J. Lehtinen, and T. Aila. Analyzing and improving the image quality of stylegan. In *Computer Society Conference on Computer Vision and Pattern Recognition (CVPR)*, pages 8110–8119, 2020.
- [29] D. P. Kingma and M. Welling. Auto-encoding variational Bayes. *International Conference on Learning Representations (ICLR)*, 2014.
- [30] A. B. L. Larsen, S. K. Sønderby, H. Larochelle, and O. Winther. Autoencoding beyond pixels using a learned similarity metric. In *International Conference on Machine Learning (ICML)*, pages 1558–1566, 2016.
- [31] I. Higgins, L. Matthey, A. Pal, C. Burgess, X. Glorot, M. Botvinick, S. Mohamed, and A. Lerchner. Beta-VAE: Learning basic visual concepts with a constrained variational framework. In *International Conference on Learning Representations (ICLR)*, volume 2, page 6, 2017.
- [32] D. Ha and J. Schmidhuber. Recurrent world models facilitate policy evolution. *Advances in Neural Information Processing Systems (NeurIPS)*, 31, 2018.
- [33] A. Xie, D. P. Losey, R. Tolsma, C. Finn, and D. Sadigh. Learning latent representations to influence multi-agent interaction. In *Conference on Robot Learning (CoRL)*, 2021.
- [34] W. Schwarting, T. Seyde, I. Gilitschenski, L. Liebenwein, R. Sander, S. Karaman, and D. Rus. Deep latent competition: Learning to race using visual control policies in latent space. In *Conference on Robot Learning (CoRL)*, 2021.
- [35] I. Lenz, R. A. Knepper, and A. Saxena. DeepMPC: Learning deep latent features for model predictive control. In *Robotics: Science and Systems*, volume 10, 2015.
- [36] N. Wahlström, T. B. Schön, and M. P. Deisenroth. From pixels to torques: Policy learning with deep dynamical models. *Deep Learning Workshop at the International Conference on Machine Learning*, 2015.
- [37] Z. Xu, Z. He, J. Wu, and S. Song. Learning 3D dynamic scene representations for robot manipulation. In *Conference on Robot Learning (CoRL)*, 2020.
- [38] S. W. Kim, J. Phillion, A. Torralba, and S. Fidler. DriveGAN: Towards a controllable high-quality neural simulation. In *Computer Society Conference on Computer Vision and Pattern Recognition (CVPR)*, pages 5820–5829, 2021.
- [39] H. Caesar, V. Bankiti, A. H. Lang, S. Vora, V. E. Liong, Q. Xu, A. Krishnan, Y. Pan, G. Baldan, and O. Beijbom. nuScenes: A multimodal dataset for autonomous driving. In *Computer Society Conference on Computer Vision and Pattern Recognition (CVPR)*, pages 11621–11631. IEEE, 2020.
- [40] P. Sun, H. Kretzschmar, X. Dotiwalla, A. Chouard, V. Patnaik, P. Tsui, J. Guo, Y. Zhou, Y. Chai, B. Caine, et al. Scalability in perception for autonomous driving: Waymo Open Dataset. In *Computer Society Conference on Computer Vision and Pattern Recognition (CVPR)*, pages 2446–2454. IEEE, 2020.
- [41] J. Dequaire, P. Ondruška, D. Rao, D. Wang, and I. Posner. Deep tracking in the wild: End-to-end tracking using recurrent neural networks. *International Journal of Robotics Research*, 37 (4-5):492–512, 2018.
- [42] P. Ondruska and I. Posner. Deep tracking: Seeing beyond seeing using recurrent neural networks. In *AAAI Conference on Artificial Intelligence (AAAI)*, 2016.

- [43] M. Jaderberg, K. Simonyan, A. Zisserman, et al. Spatial transformer networks. *Advances in Neural Information Processing Systems (NeurIPS)*, 28, 2015.
- [44] W. Lotter, G. Kreiman, and D. Cox. Deep predictive coding networks for video prediction and unsupervised learning. In *International Conference on Learning Representations (ICLR)*, 2017.
- [45] P. Baldi and K. Hornik. Neural networks and principal component analysis: Learning from examples without local minima. *Neural Networks*, 2(1):53–58, 1989.
- [46] G. E. Hinton. Connectionist learning procedures. In *Machine Learning*, pages 555–610. Elsevier, 1990.
- [47] G. E. Hinton and R. Zemel. Autoencoders, minimum description length and Helmholtz free energy. *Advances in Neural Information Processing Systems (NeurIPS)*, 6, 1993.
- [48] L. Buesing, T. Weber, S. Racaniere, S. Eslami, D. Rezende, D. P. Reichert, F. Viola, F. Besse, K. Gregor, D. Hassabis, and D. Wierstra. Learning and querying fast generative models for reinforcement learning. *FAIM Workshop on Prediction and Generative Modeling in Reinforcement Learning*, 2018.
- [49] D. Hafner, T. Lillicrap, I. Fischer, R. Villegas, D. Ha, H. Lee, and J. Davidson. Learning latent dynamics for planning from pixels. In *International Conference on Machine Learning (ICML)*, 2019.
- [50] C. Gelada, S. Kumar, J. Buckman, O. Nachum, and M. G. Bellemare. DeepMDP: Learning continuous latent space models for representation learning. In *International Conference on Machine Learning (ICML)*, pages 2170–2179, 2019.
- [51] D. Hafner, T. Lillicrap, J. Ba, and M. Norouzi. Dream to control: Learning behaviors by latent imagination. In *International Conference on Learning Representations (ICLR)*, 2019.
- [52] T. Kurutach, A. Tamar, G. Yang, S. J. Russell, and P. Abbeel. Learning plannable representations with causal InfoGAN. *Advances in Neural Information Processing Systems (NeurIPS)*, 31, 2018.
- [53] A. Anand, E. Racah, S. Ozair, Y. Bengio, M.-A. Côté, and R. D. Hjelm. Unsupervised state representation learning in Atari. *Advances in Neural Information Processing Systems (NeurIPS)*, 32, 2019.
- [54] T. Z. Zhao, A. Nagabandi, K. Rakelly, C. Finn, and S. Levine. MELD: Meta-reinforcement learning from images via latent state models. In *Conference on Robot Learning (CoRL)*, 2021.
- [55] W. Zhou, S. Bajracharya, and D. Held. PLAS: Latent action space for offline reinforcement learning. In *Conference on Robot Learning (CoRL)*, 2021.
- [56] J. Sohl-Dickstein, E. Weiss, N. Maheswaranathan, and S. Ganguli. Deep unsupervised learning using nonequilibrium thermodynamics. In *International Conference on Machine Learning (ICML)*, pages 2256–2265, 2015.
- [57] J. Ho, A. Jain, and P. Abbeel. Denoising diffusion probabilistic models. *Advances in Neural Information Processing Systems (NeurIPS)*, 33:6840–6851, 2020.
- [58] J. Song, C. Meng, and S. Ermon. Denoising diffusion implicit models. In *International Conference on Learning Representations (ICLR)*, 2021.
- [59] J. Ho, T. Salimans, A. A. Gritsenko, W. Chan, M. Norouzi, and D. J. Fleet. Video diffusion models. In *ICLR Workshop on Deep Generative Models for Highly Structured Data*, 2022.

- [60] M. Babaeizadeh, C. Finn, D. Erhan, R. H. Campbell, and S. Levine. Stochastic variational video prediction. In *International Conference on Learning Representations (ICLR)*, 2018.
- [61] A. X. Lee, R. Zhang, F. Ebert, P. Abbeel, C. Finn, and S. Levine. Stochastic adversarial video prediction. *Computing Research Repository (CoRR)*, 2018.
- [62] D. Weissenborn, O. Täckström, and J. Uszkoreit. Scaling autoregressive video models. In *International Conference on Learning Representations (ICLR)*, 2020.
- [63] L. Yu, Y. Cheng, K. Sohn, J. Lezama, H. Zhang, H. Chang, A. G. Hauptmann, M.-H. Yang, Y. Hao, I. Essa, et al. Magvit: Masked generative video transformer. In *Computer Society Conference on Computer Vision and Pattern Recognition (CVPR)*, pages 10459–10469, 2023.
- [64] A. Vaswani, N. Shazeer, N. Parmar, J. Uszkoreit, L. Jones, A. N. Gomez, L. Kaiser, and I. Polosukhin. Attention is all you need. In *Advances in Neural Information Processing Systems (NeurIPS)*, pages 5998–6008, 2017.
- [65] R. Zhang, P. Isola, A. A. Efros, E. Shechtman, and O. Wang. The unreasonable effectiveness of deep features as a perceptual metric. In *Computer Society Conference on Computer Vision and Pattern Recognition (CVPR)*, pages 586–595, 2018.
- [66] P. Isola, J.-Y. Zhu, T. Zhou, and A. A. Efros. Image-to-image translation with conditional adversarial networks. In *Computer Society Conference on Computer Vision and Pattern Recognition (CVPR)*, pages 1125–1134, 2017.
- [67] E. Denton and R. Fergus. Stochastic video generation with a learned prior. In *International Conference on Machine Learning (ICML)*, pages 1174–1183, 2018.
- [68] J.-Y. Franceschi, E. Delasalles, M. Chen, S. Lamprier, and P. Gallinari. Stochastic latent residual video prediction. In *International Conference on Machine Learning (ICML)*, pages 3233–3246, 2020.
- [69] T.-C. Wang, M.-Y. Liu, J.-Y. Zhu, G. Liu, A. Tao, J. Kautz, and B. Catanzaro. Video-to-video synthesis. In *Advances in Neural Information Processing Systems (NeurIPS)*, 2018.
- [70] T. R. Shaham, T. Dekel, and T. Michaeli. Singan: Learning a generative model from a single natural image. In *Computer Society Conference on Computer Vision and Pattern Recognition (CVPR)*, pages 4570–4580, 2019.
- [71] A. Paszke, S. Gross, F. Massa, A. Lerer, J. Bradbury, G. Chanan, T. Killeen, Z. Lin, N. Gimelshein, L. Antiga, et al. PyTorch: An imperative style, high-performance deep learning library. In *Advances in Neural Information Processing Systems (NeurIPS)*, pages 8026–8037, 2019.
- [72] W. Falcon and The PyTorch Lightning team. PyTorch Lightning, Mar. 2019. URL <https://github.com/Lightning-AI/lightning>.
- [73] I. Loshchilov and F. Hutter. Decoupled weight decay regularization. In *International Conference on Learning Representations (ICLR)*, 2019.
- [74] Z. Gao, C. Tan, L. Wu, and S. Z. Li. Simvp: Simpler yet better video prediction. In *Computer Society Conference on Computer Vision and Pattern Recognition (CVPR)*, pages 3170–3180, 2022.
- [75] Y. Wang, H. Wu, J. Zhang, Z. Gao, J. Wang, S. Y. Philip, and M. Long. Predrnn: A recurrent neural network for spatiotemporal predictive learning. *IEEE Transactions on Pattern Analysis and Machine Intelligence*, 45(2):2208–2225, 2022.

- [76] Y. Wang, L. Jiang, M.-H. Yang, L.-J. Li, M. Long, and L. Fei-Fei. Eidetic 3d lstm: A model for video prediction and beyond. In *International Conference on Learning Representations (ICLR)*, 2019.
- [77] A. Birk and S. Carpin. Merging occupancy grid maps from multiple robots. *Proceedings of the IEEE*, 94(7):1384–1397, 2006.
- [78] M. Itkina and M. J. Kochenderfer. Interpretable self-aware neural networks for robust trajectory prediction. In *Conference on Robot Learning (CoRL)*, 2022.
- [79] M. Itkina, Y.-J. Mun, K. Driggs-Campbell, and M. J. Kochenderfer. Multi-agent variational occlusion inference using people as sensors. In *International Conference on Robotics and Automation (ICRA)*. IEEE, 2022.
- [80] A. Dosovitskiy, G. Ros, F. Codevilla, A. Lopez, and V. Koltun. CARLA: an open urban driving simulator. In *Conference on Robot Learning (CoRL)*, pages 1–16, 2017.

A Hyperparameteres

A.1 Encoder & Decoder

Table 3: Representation Learning Hyperparameters

Parameter	Value
Architecture	ResNet
Image Size	$1 \times 128 \times 128$
Latent Dim L-OGM	$64 \times 4 \times 4$
Latent Dim Camera	$16 \times 4 \times 4$
Latent Dim Maps	$16 \times 4 \times 4$
Channel Multiplier	2
Optimizer	Adam(lr=0.0001)
Batch size	24 per GPU
KL reg β	50.0
Adv weight γ	1.0
Path reg	2.0
Discriminator R1 reg	10.0
GPUS	4 NVIDIA V100 32 GB

A.2 Prediction Network

Table 4 contains the hyperparameters for stochastic prediction. The prediction network training consists of three stages: deterministic training, low regularization training, and high regularization training. During deterministic training stage, z_{stoch} is sampled from the target distribution. During regularized training, z_{stoch} is sampeld from the inference network.

Table 4: Stochastic Prediction Hyperparameters

Parameter	Value
Architecture	Transformer
d_{embed}	256
N_{enc}	2
N_{dec}	1
N_{heads}	2
$d_{feedforward}$	128
Dropout	0.01
Optimizer	AdamW(lr=0.0004)
Deterministic Epochs	10
Low Reg Epochs	10
KL reg low γ	0.0001
KL reg γ	0.001
GPU	1 NVIDIA RTX TITAN 24 GB

B Image Similarity Metric

The Image Similarity metric determines the picture distance function ψ between two matrices m_1 and m_2 as follows [77]:

$$\psi(m_1, m_2) = \sum_{c \in \mathcal{C}} d(m_1, m_2, c) + d(m_2, m_1, c) \quad (6)$$

where

$$d(m_1, m_2, c) = \frac{\sum_{m_1[p]=c} \min\{\text{md}(p_1, p_2) | m_2[p_2] = c\}}{\#_c(m_1)}. \quad (7)$$

\mathcal{C} is a set of discretized values assumed by m_1 or m_2 which are: occupied, occluded, and free. $m_1[p]$ denotes the value c of map m_1 at position $p = (x, y)$. $\text{md}(p_1, p_2) = |x_1 - x_2| + |y_1 - y_2|$ is the Manhattan distance between points p_1 and p_2 . $\#_c(m_1) = \#\{p_1 \mid m_1[p_1] = c\}$ is the number of cells in m_1 with value c .

C Additional Qualitative Results

Figure 6 compares VAE-GAN (used in our experiments) and VAE. Samples from VAE-GAN appear more realistic and have sharper occupied cells. Besides the qualitative preferences, the choice of representation learning framework does not translate to significant quantitative differences.

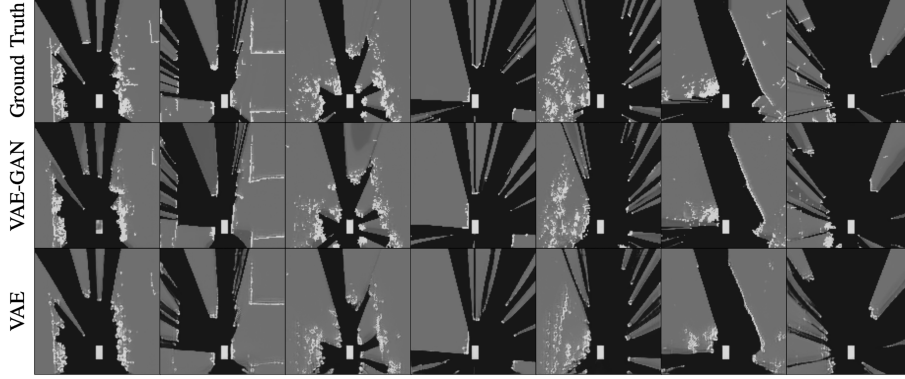


Figure 6: Comparison between VAE-GAN and VAE on Nuscenes.